p-$HOC_6H_4O^{\bullet}$, 3225-30-7; o-$MeOC_6H_4O^{\bullet}$, 41115-74-6; p-$MeOC_6H_4O^{\bullet}$, 6119-32-0; o-$ClC_6H_4O^{\bullet}$, 63125-12-2; p-$PhC_6H_4O^{\bullet}$, 35645-18-2; o-$MeC_6H_4O^{\bullet}$, 3174-49-0; p-$BrC_6H_4O^{\bullet}$, 63125-13-3; p-$ClC_6H_4O^{\bullet}$, 3148-13-8; p-t-$BuC_6H_4O^{\bullet}$, 35645-16-0; p-$MeC_6H_4O^{\bullet}$, 3174-48-9; p-$O_2NC_6H_4O^{\bullet}$, 41071-23-2; p-$PhCOC_6H_4O^{\bullet}$, 131761-88-1; p-$AcC_6H_4O^{\bullet}$, 54560-34-8; p-$NCC_6H_4O^{\bullet}$, 41071-24-3; p-$PhSO_2C_6H_4O^{\bullet}$, 131588-31-3; p-$F_3CC_6H_4O^{\bullet}$, 73073-68-4; PhOH (radical cation), 40932-22-7; o-MeC_6H_4OH (radical cation), 60715-73-3; m-MeC_6H_4OH (radical cation), 60715-74-4; p-MeC_6H_4OH (radical cation), 51921-65-4; p-t-BuC_6H_4OH (radical cation), 122060-12-2; p-PhC_6H_4OH (radical cation), 58587-96-5; o-$MeOC_6H_4OH$ (radical cation), 60715-77-7; m-$MeOC_6H_4OH$ (radical cation), 60715-78-8; p-$MeOC_6H_4OH$ (radical cation), 34471-10-8; p-HOC_6H_4OH (radical cation), 34507-04-5; m-$NH_2C_6H_4OH$ (radical cation), 34478-00-7; m-$Me_2NC_6H_4OH$ (radical cation), 131588-33-5; p-$H_2NC_6H_4OH$ (radical cation), 60715-76-6; p-$Me_2NC_6H_4OH$ (radical cation), 131588-34-6; o-ClC_6H_4OH (radical cation), 73073-76-4; m-ClC_6H_4OH (radical cation), 73073-75-3; p-ClC_6H_4OH (radical cation), 73073-74-2; p-BrC_6H_4OH (radical cation), 80173-15-5; m-$F_3CC_6H_4OH$ (radical cation), 73073-71-9; p-$F_3CC_6H_4OH$ (radical cation), 73073-69-5; m-$MeSO_2C_6H_4OH$ (radical cation), 131588-37-9; p-$MeSO_2C_6H_4OH$ (radical cation), 131588-38-0; m-AcC_6H_4OH (radical cation), 73073-63-9; p-AcC_6H_4OH (radical cation), 73073-62-8; p-$PhCOC_6H_4OH$ (radical cation), 131588-39-1; m-NCC_6H_4OH (radical cation), 131588-40-4; p-NCC_6H_4OH (radical cation), 131588-41-5; m-$O_2NC_6H_4OH$ (radical cation), 73089-74-4; p-$O_2NC_6H_4OH$ (radical cation), 73089-73-3; 3,5-dimethylphenol, 108-68-9; 2,6-diethylphenol, 576-26-1; 2,6-di-*tert*-butylphenol, 128-39-2; 2,4,6-tri-*tert*-butylphenol, 732-26-3; 3,5-dichlorophenol, 591-35-5; 3,4,5-trichlorophenol, 609-19-8; 2-naphthol, 135-19-3; 6-bromo-2-naphthol, 15231-91-1; 1-naphthol, 90-15-3; 2,6-di-*tert*-butylphenoxy radical, 15773-11-2; 3,4,5-trichlorophenoxy radical, 131761-87-0; 2,6-dimethoxyphenoxy radical, 3229-35-4; 3,5-dimethylphenol radical cation, 73073-77-5; 2,6-dimethylphenol radical cation, 131588-32-4; 2,6-di-*tert*-butylphenol radical cation, 42150-58-3; 2,4,6-tri-*tert*-butylphenol radical cation, 42150-54-9; 3,5-dichlorophenol radical cation, 131588-35-7; 3,4,5-trichlorophenol radical cation, 131588-36-8; 1-naphthol radical cation, 72773-99-0; 6-bromo-2-naphthol radical cation, 131588-42-6; 2-naphthol radical cation, 67977-56-4.

[3]Rotane: Crystal Structure, X–X Difference Electron Density, and Phase Transition†

Roland Boese,*[1a] Thomas Miebach,[1a] and Armin de Meijere[1b]

Contribution from the Institut für Anorganische Chemie, Universität Essen-GH, D-4300 Essen 1, FR Germany, and Institut für Organische Chemie, Universität Hamburg, D-2000 Hamburg 13, FR Germany. *Received August 9, 1990*

Abstract: The newly redetermined X-ray crystal structure of [3]rotane (**1**) provides structural parameters in close agreement with theoretical calculations. In relation to cyclopropane, a shortening of the vicinal bonds at the spiro carbon atoms and a lengthening of the distal bonds is observed. The latter is apparently due to the increased angular strain at the spiro carbon atoms. In a series of spiro[2.n]alkanes the angle in the (n+1)-membered ring correlates inversely with the length of the distal bond in the cyclopropane group. The determined X–X difference electron density for **1** strongly corroborates the theoretically predicted surface delocalization of electrons in three-membered rings; this adds an essential argument in favor of the concept of "σ-aromaticity". Upon cooling, the crystal of **1** undergoes a reversible phase transition at 108.2 K. Crystal symmetry changes from space group $P6_3/m$ to $P2_1/n$. Structural and cell parameters were determined at different temperatures to understand this molecular reorganization. Most probably the increasing number of van der Waals contacts in the low-temperature form provides the driving force for the phase transition.

Introduction

As the most highly strained member in the [n]rotane series, [3]rotane (**1**)[2] has been the object of considerable research effort.

Calculations to evaluate the hybridization of the spiro carbon atoms were reported by Randić et al. and by Maksić et al.[3] [3]Rotane (**1**) was first synthesized by Fitjer and Conia[4] in 1973; a different synthesis was later developed by Erden et al.[5] Photoelectron spectroscopy revealed an unusually large resonance integral between the spirocyclopropane groups in **1**.[6] Semiempirical calculations (MINDO/3) were carried out by Zil'berg et al.[7] to evaluate the geometry and strain energy of **1**. Other theoretical methods were applied by Rasmussen and Tosi[8] (consistent force field calculation) and by Ioffe et al.[9] (molecular mechanics calculation). Except for the MINDO/3 method, all theoretical calculations for **1** predict a lengthening of the distal bond c relative to the proximal bond b and the central bond a (Figure 1). The distal bond lengthening apparently would result from a partial release of the additional angle strain at the spiro atoms. These reasonable theoretical results contradict the experimentally derived parameters from an X-ray crystal structure analysis at 228 K.[10]

Results

In order to resolve this discrepancy we redetermined the X-ray crystal structure of **1** at 120 K. Furthermore, the X–X difference electron density was evaluated to verify the predicted surface delocalization of σ-electrons in cyclopropane and its derivatives.[11] On cooling, the crystal undergoes a reversible phase transition with a change of crystal symmetry. In order to understand this

† Dedicated to Prof. B. Schrader on the occasion of his 60th birthday.

(1) (a) Universität-GH Essen. (b) Universität Hamburg, new address: Institut für Organische Chemie, Georg-August-Universität, Tammannstrasse 2, D-3400 Göttingen, FR Germany.

(2) The systematic name of [3]rotane is trispiro[2.0.2.0.2.0]nonane.

(3) (a) Randić, M.; Jacab, L. *Croat. Chim. Acta* **1971**, *42*, 425. (b) Randić, M.; Kumar, L. *J. Mol. Struct.* **1975**, *26*, 145. (c) Kovačević, K.; Maksić, Z. B.; Moguš, A. *Croat. Chim. Acta* **1979**, *52*, 249. (d) Maksić, Z. B.; Eckert-Maksić, M.; Rupnik, K. *Croat. Chim. Acta* **1984**, 1295.

(4) (a) Randić, M.; Fitjer, L.; Conia, J.-M. *Angew. Chem.* **1973**, *85*, 349; *Angew. Chem., Int. Ed. Engl.* **1973**, *12*, 332. (b) Cf. also: Fitjer, L. *Chem. Ber.* **1982**, *115*, 1047 and references cited therein.

(5) Erden, I. *Synth. Commun.* **1986**, *16*, 117.

(6) Gleiter, R.; Haider, R.; Conia, J.-M.; Barnier, J.-P.; de Meijere, A.; Weber, W. *J. Chem. Soc., Chem. Commun.* **1979**, 130.

(7) Zil'berg, S. P.; Ioffe, A. I.; Nefedov, O. M. *Izv. Akad. Nauk SSSR, Ser. Khim.* **1983**, *2*, 261.

(8) Rasmussen, K.; Tosi, C. *J. Mol. Struct. (Theochem)* **1985**, *121*, 233.

(9) Ioffe, A. I.; Svyatkin, V. A.; Nefedov, O. M. *Izv. Akad. Nauk SSSR, Ser. Khim.* **1987**, *4*, 801.

(10) (a) Pascard, C.; Prangé, T.; de Meijere, A.; Weber, W.; Barnier, J.-P.; Conia, J.-M. *J. Chem. Soc., Chem. Commun.* **1979**, *9*, 425. (b) Prangé, T.; Pascard, C.; de Meijere, A.; Behrens, U.; Barnier, J.-P.; Conia, J.-M. *Nouv. J. Chim.* **1980**, *4*, 321. (c) The bond lengths and angles given in refs a and b differ from the corresponding parameters as calculated from the listed atomic coordinates.

(11) Cremer, D. *Tetrahedron* **1988**, *44*, 7427 and references cited therein.

0002-7863/91/1513-1743$02.50/0

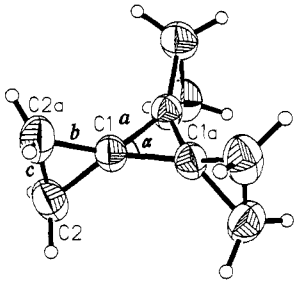

Figure 1. Presentation of **1** with thermal probability plots of 50%. Bond lengths and libration corrected bond lengths (in parentheses): 1.475 (2) Å (1.480 Å) for the central ring bond a, 1.477 (1) Å (1.478 Å) for the vicinal bond b, and 1.525 (2) Å (1.529 Å) for the distal bond c.

Table I. List of Cell Dimensions[a]

T (K)	a (Å)	b (Å)	c (Å)	V [Å^3]
96[b]	6.582 (4)	9.655 (5)	11.700 (5)	743.6 (6)
100[b]	6.584 (3)	9.656 (4)	11.700 (5)	743.9 (5)
105[b]	6.587 (3)	9.654 (4)	11.701 (6)	744.1 (5)
110	6.748 (1)	6.748 (1)	9.431 (2)	372.0 (1)
115	6.748 (1)	6.748 (1)	9.433 (2)	372.0 (1)
120	6.749 (1)	6.749 (1)	9.442 (2)	372.5 (2)
130	6.752 (1)	6.752 (1)	9.457 (2)	373.5 (1)
140	6.756 (1)	6.756 (1)	9.478 (2)	374.7 (2)
150	6.759 (1)	6.759 (1)	9.498 (2)	375.8 (1)
160	6.763 (1)	6.763 (1)	9.514 (2)	376.9 (1)
170	6.767 (1)	6.767 (1)	9.530 (2)	377.9 (2)
180	6.771 (1)	6.771 (1)	9.545 (2)	379.1 (2)
190	6.776 (1)	6.776 (1)	9.562 (2)	380.2 (2)
200	6.780 (1)	6.780 (1)	9.578 (2)	381.3 (2)
210	6.783 (1)	6.783 (1)	9.595 (2)	382.3 (1)
220	6.788 (1)	6.788 (1)	9.610 (2)	383.5 (1)

[a] All cells hexagonal except the monoclinic cells at 96, 100, and 105 K. [b] Monoclinic angles: 96 K, 90.49 (6)°; 100 K, 91.26 (4)°; 105 K, 90.27 (4)°.

phase transition, the crystal structures and cell dimensions were determined at different temperatures.

Experimental Section

(a) Crystal Structure at 120 K. The crystal (0.25 × 0.25 × 0.30 mm^3) was grown by sublimation at 279 K. Data were collected on a Nicolet R3m/V X-ray diffractometer with Mo Kα (λ = 0.71069 Å) radiation at T = 120 K. With diffractometer angles of 32 reflections (20° ≤ 2θ ≤ 25°) the hexagonal cell was refined yielding $a = b$ = 6.7491 (12) Å, c = 9.442 (2) Å, $\alpha = \beta$ = 90°, γ = 120°, V = 372.5 (2) Å^3, Z = 2, ρ_{calc} = 1.072 g cm^3, space group $P6_3/m$ [ω-scan data collection (scan range 1.20°), 2399 intensities were measured (3° ≤ 2θ ≤ 60°), 395 merged reflections (R_{merg} = 0.0123), 377 of which were treated as observed ($F_o \geq 4.0\,\sigma(F)$), no absorption correction applied (μ = 0.06 cm^{-1}), extinction correction according to $F_c^* = F_c(1-10^{-6} \times F_c^2/\sin\Theta)$]. The structure was solved by direct methods and refined in the full matrix (R = 0.039, R_w = 0.041, 25 parameters) with SHELXTL-PLUS (Vers. 4.0) on a MicroVAX IIa. Atom scattering factors were taken from Cromer and Mann.[12] Figure 1 shows the thermal ellipsoid plot of **1**.

(b) X-X Difference Electron Density. Additional reflections were measured in the range of 60° ≤ 2θ ≤ 90°; 4115 intensities were merged into 1077 unique reflections (R_{merg} = 0.0093), 904 of which were treated as observed ($F_o \geq 4.0\sigma(F)$). After the last refinement cycle, applying a weighing scheme $w = -\exp(-5 \times (\sin(\Theta)/\lambda)^2)$ and fixed hydrogen positions (R = 0.044, R_w = 0.044) the atom positions of the hydrogen atoms were shifted to a C–H distance of 1.08 Å from their previously refined positions. The difference electron density was calculated with SHELXTL. Figure 2a shows the difference electron density within the plane defined by the three atoms of the central ring (C1, C1a, C1b); Figure 2b shows the difference electron density in the plane of the outer ring (C1, C2, C2a).

(c) Phase Transition. The first indication of a phase transition was obtained from the fact that some of the reflections vanished on cooling the crystal on the diffractometer. As the DSC thermogram indicates, the fully reversible phase transition occurs at 108.2 K on cooling and at 117.6 K on heating (−0.369 kJ/mol) (see Figure 3). The melting point

(12) Cromer, D. T.; Mann, J. B. *Acta Crystallogr.* **1968**, *A24*, 321.

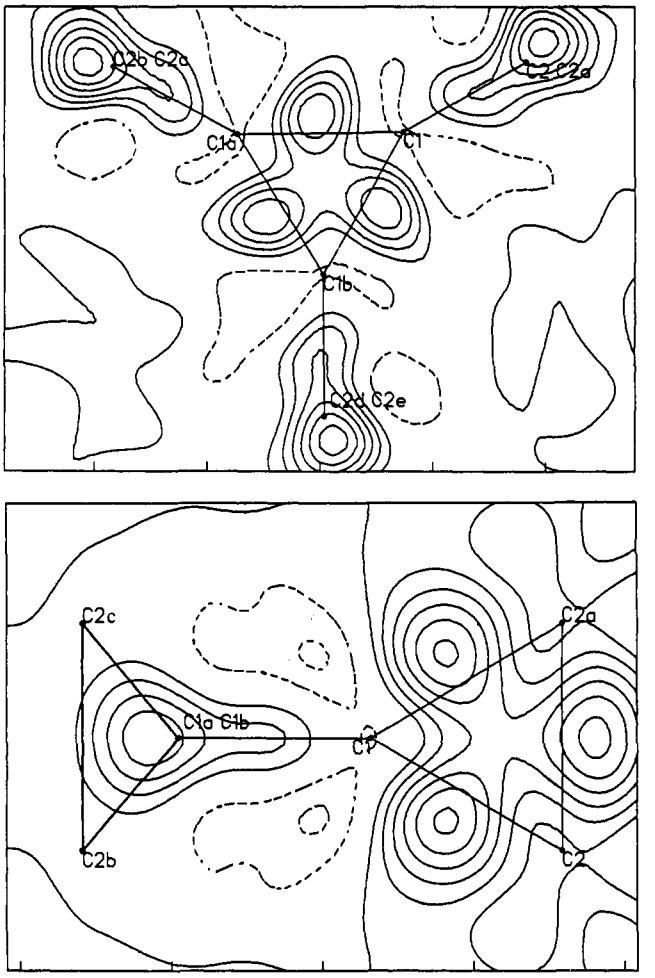

Figure 2. Presentation of X–X electron densities with a distance of 0.05 e/Å^3 (positive and zero, solid lines) and 0.1 e/Å^3 (negative, dotted lines): top (a) section within the central ring plane and bottom (b) section within the plane of the outer ring.

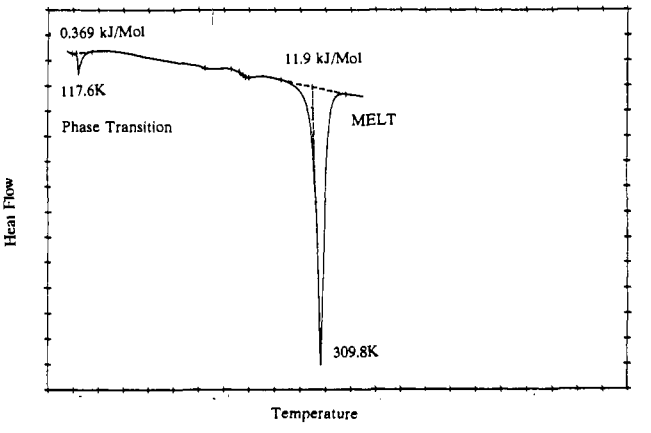

Figure 3. DSC curve of **1** on heating.

was found to be 309.8 K (−11.9 kJ/mol).

Changes of cell dimensions also reflect this phase transition. For comparison, the cell dimensions were transformed from hexagonal to monoclinic symmetry and scaled to the cell dimensions at 120 K. According to the temperature dependence of the scaled cell dimensions (see Figure 4), phase transition occurs somewhere in the temperature range between 110 and 96 K on cooling. In the high-temperature phase (HT-phase), the cell dimensions follow a strict linear temperature dependence from 220 to 110 K (see Figure 4 and Table I).

The molecular structure was determined at seven different temperatures with the low-temperature phase (LT-phase) assigned to the space group $P2_1/n$ and the HT-phase to $P6_3/m$. The experimental data are listed in Table II, and tables for atomic positions and thermal parameters

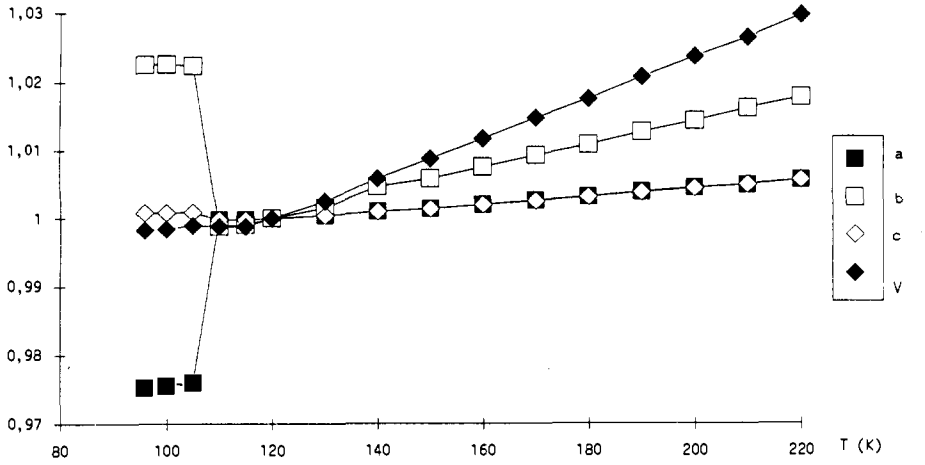

Figure 4. Cell dimensions of [3]rotane (**1**) as a function of temperature, scaled to the values at 120 K and all transformed from hexagonal to monoclinic symmetry for reasons of better comparison (transformation matrix 0 −1 0 / 0 0 1 / −2 −1 0).

Table II. Number of Measured, Merged, and Observed Intensities, Number of Parameters, R Value, Weighted R Value, and Merging R Value[a]

T (K)	n_{meas}	n_{merg}	R_{merg}	n_{obs}	n_{param}	R	R_w
96	2531	1298	0.053	1142	88	0.080	0.086
120	2399	395	0.012	377	25	0.039	0.041
140	2293	399	0.012	386	25	0.042	0.044
160	1269	400	0.014	357	25	0.039	0.040
180	1269	400	0.013	351	25	0.043	0.043
200	1269	400	0.013	347	25	0.044	0.044
220	1283	404	0.011	343	25	0.045	0.045

[a] $R = \sum||F_o| - |F_c||/\sum|F_o|$, $R_w = [\sum w||F_o| - |F_c||^2/\sum w|F_o|^2]^{1/2}$, $w^{-1} = \sigma^2(F_o) + g^*F_o^2$.

Table III. Observed and Libration Corrected Bond Lengths for **1** at Different Temperatures[a]

	a (Å)		b (Å)		c (Å)	
T (K)	uncorr	corr	uncorr	corr	uncorr	corr
96	1.486 (3)	1.488	1.476 (3)	1.477	1.531 (2)	1.533
120	1.475 (2)	1.480	1.477 (1)	1.478	1.525 (2)	1.529
140	1.474 (2)	1.478	1.475 (2)	1.477	1.522 (2)	1.526
160	1.475 (2)	1.476	1.473 (2)	1.479	1.518 (2)	1.522
180	1.474 (2)	1.476	1.472 (2)	1.478	1.515 (2)	1.521
200	1.474 (2)	1.475	1.470 (2)	1.479	1.512 (2)	1.518
220	1.472 (2)	1.475	1.470 (2)	1.477	1.510 (2)	1.517

[a] Bond lengths at 96 K merged to C_{2v} symmetry.

for the LT-phase are available as supplementary material.

Because of the high symmetry and rigidity of the molecule no significant change in molecular structure occurs (see Table III). The slight temperature dependence of the corrected bond lengths[13] is probably caused by an inadequate libration correction. Figure 5a–d show the thermal ellipsoid plots of **1** at four different temperatures.

The temperature dependence of thermal parameters of carbon atoms is shown in Figure 6a,b. All thermal parameters of the HT-phase follow a linear temperature dependence from 220 to 110 K. Illustrations of the cell contents in both phases are given in Figures 7a–c and 8a–c for the HT-phase at 120 K and the LT-phase at 96 K, respectively.

The HT-phase consists of layers of coplanar molecules arranged around the 3-fold axis. In the zigzag layers of the LT-phase, the molecules are alternately tilted by 10.6°. The axis of tilting is parallel to the c-axis of the cell. The zigzag layers require more space in the b-axis. In the direction of the a-axis, a denser packing of the molecules is reflected by a shorter a-axis compared with the HT-phase. The c-axis, parallel to the axis of tilting, remains almost unchanged.

Discussion

(a) Crystal Structure of 1 at 120 K. The molecule of [3]rotane (**1**) as shown in Figure 1 reveals the expected D_{3h} symmetry according to the space group $P6_3/m$. The space group is the same as that found by Prangé et al., only the cell dimensions are slightly different because of the lower temperature used in this determination (120 K instead of 228 K). But the bond lengths differ substantially from those reported by Prangé et al. The following discussions will therefore refer to our own more precise data. The finding that the distal bond c is longer than the proximal bonds a and b is in accord with theoretical predictions except for the MINDO/3 calculation,[14] although absolute values are different, see Table IV.

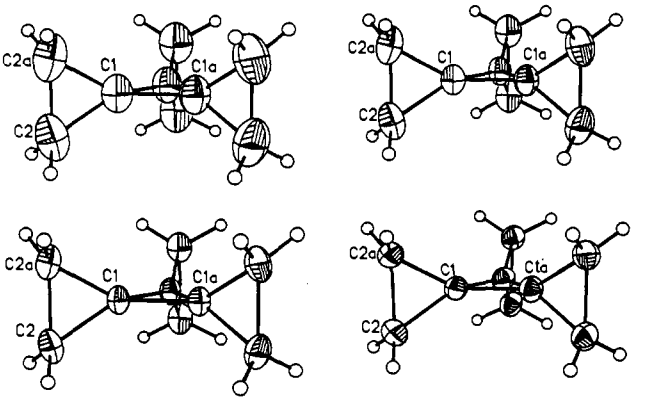

Figure 5. Presentation of **1** as thermal probability plots of 50% at four different temperatures: top left (a) 220 K, top right (b) 160 K, bottom left (c) 120 K, bottom right (d) 96 K.

Table IV. Comparison of Bond Lengths in **1** According to Theoretical Calculations and Experimental Investigations

method of investigation	length of C–C bonds (Å)		
	a	b	c
MINDO/3	1.510	1.506	1.489
CFF:PEF304	1.519	1.478	1.598
PEF404	1.504	1.483	1.555
MM/2	1.475	1.477	1.538
AM1	1.465	1.483	1.507
IMO[3c]	1.468	1.494	1.520
MNDO	1.495	1.510	1.530
X-ray			
Prangé et al.[10b]	1.465 (4)	1.500 (4)	1.496 (4)
this work	1.475 (2)	1.477 (1)	1.525 (2)

The lengthening of bond c can be explained by comparison with corresponding parameters in other spiro compounds. The smallest spiro[n,m]alkane, spiropentane (**2**) has been investigated by Boese et al.[15] The low-temperature X-ray crystal structure analysis

(13) Schomaker, V.; Trueblood, K. N. *Acta Crystallogr.* **1968**, *B24*, 63.

(14) Zil'berg et al.[7] explained the unusually short distal bond c with the underestimation of the strain at the spiro atoms by the MINDO/3 method.

(15) Boese, R.; Bläser, D.; Gomann, K.; Brinker, U. H. *J. Am. Chem. Soc.* **1989**, *111*, 1501.

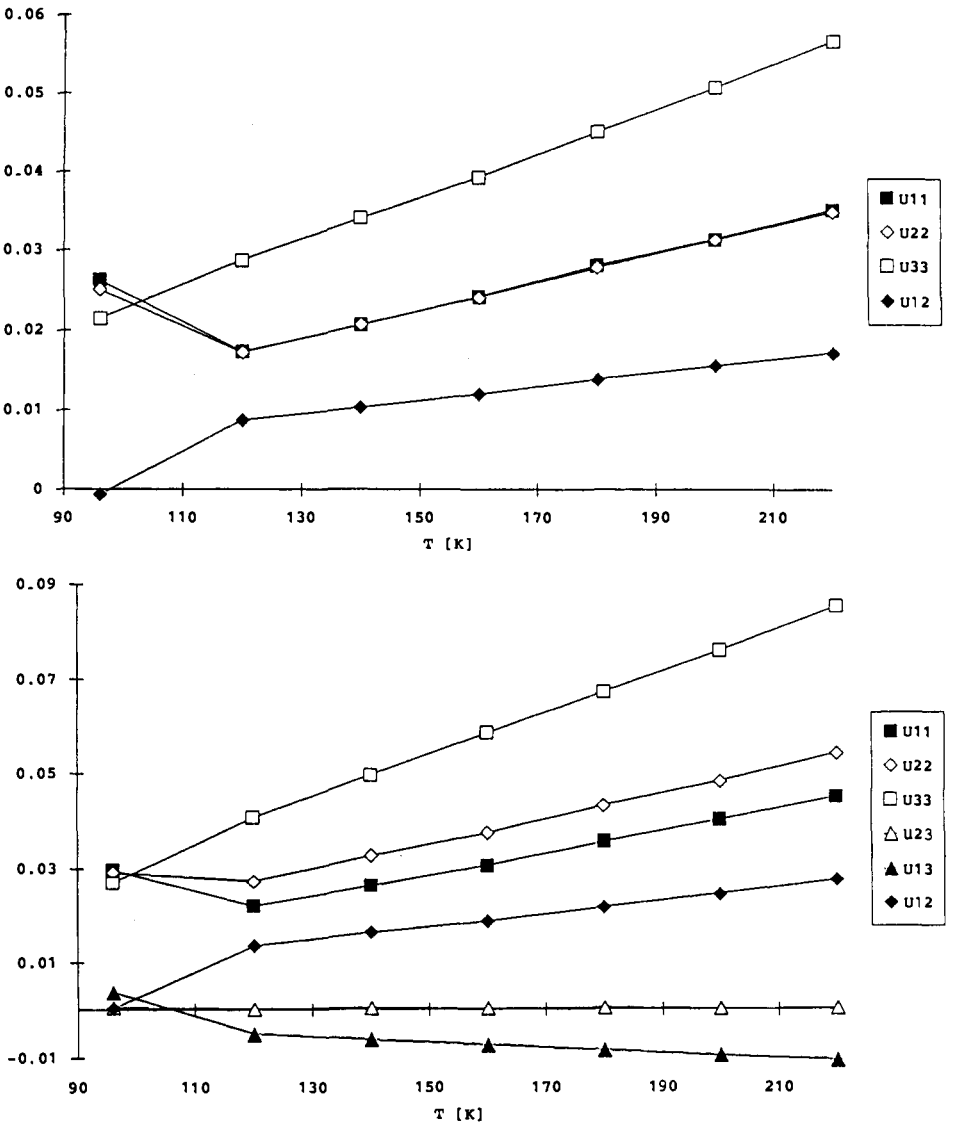

Figure 6. Temperature diagram of anisotropic thermal parameters on cooling: top (a) carbon atom of central ring (C1) and bottom (b) carbon atom of outer ring (C2).

Table V. Comparison of Bond Lengths and Angles in Different Spirocyclopropane Compounds[a]

compound	bond angle (deg) α	bond length (Å) a	b	c
methylenecyclopropane (**6**)[20]	0.0	C=C: 1.316	1.461	1.526
[3]rotane (**1**)	60.0	1.475	1.477	1.525
spiropentane (**2**)[15]	62.3	1.477	1.477	1.527
[4]rotane (**3**)[17]	90.0	1.520	1.498	1.527
[5]rotane (**4**)[10b]	103.1–105.7	1.496–1.530	1.498–1.520	1.500–1.511
[6]rotane (**5**)[10b]	111.5	1.514	1.508	1.498

[a] For the designation of a, b, c refer to Scheme I.

of **2** at 110 K reveals the distal bond as 1.527 (1) Å (1.536 Å, after libration correction), almost the same as that in **1**. In the [*n*]rotane series (n = 3, 4, 5, 6) (see Chart I) the lengths of the distal cyclopropane bonds in [4]rotane (**3**)[16,17] were found to be the same as those in **1**. [5]- (**4**) and [6]rotane (**5**),[10,18] however, show significantly shorter distal bonds in their spirocyclopropane groups. This indicates that the lengthening of the distal bond c in **1** decreases the angle strain at the spiro atom caused by the small angle which for symmetry reasons is held at 60° in the central ring. The length for the corresponding distal bond c in a less strained system like 1,1-dimethylcyclopropane has been calculated by Cremer and Kraka[19] to be 1.504 Å; this would correspond to an angle of 114.2°, if the *gem*-dimethyl groups were methylene groups as part of the cycle. Increasing the strain at the spiro atom by decreasing this angle causes lengthening of bond c. In [4]rotane (**3**), apparently the limiting value is achieved. A further decrease of the central angle does not effect the length of c. Even in methylenecyclopropane (**6**) (low-temperature X-ray crystal structure at 126 K by Boese and co-workers[20]) with a

(16) The systematic name of [4]rotane is tetraspiro[2.0.2.0.2.0.2.0]dodecane.
(17) Almenningen, A.; Bastiansen, O.; Cyvin, B. N.; Cyvin, S.; Fernholt, L.; Rømming, C. *Acta Chem. Scand.* **1984**, *A38*, 31.
(18) The systematic name of [5]rotane is pentaspiro[2.0.2.0.2.0.2.0.2.0]pentadecane, that of [6]rotane is hexaspiro[2.0.2.0.2.0.2.0.2.0.2.0]octadecane.
(19) Cremer, D.; Kraka, E. *J. Am. Chem. Soc.* **1985**, *107*, 3811.
(20) Boese, R.; Bläser, D.; Niederprüm, N. To be published.

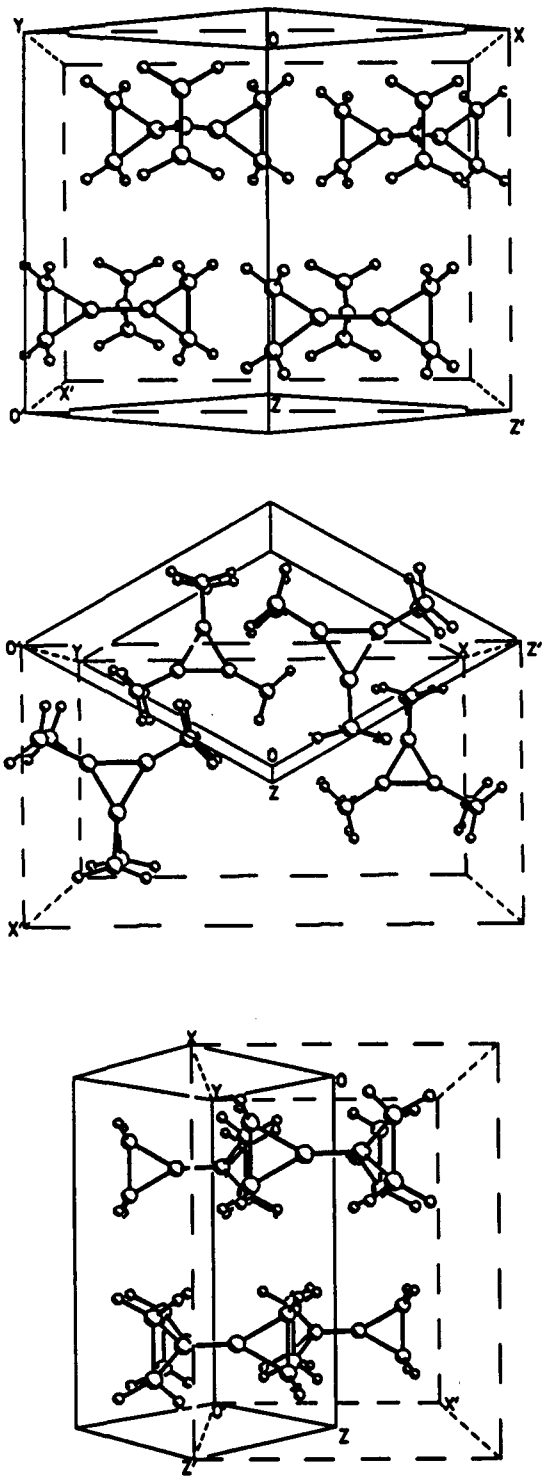

Figure 7. Cell contents of the 120 K HT-phase. Dotted lines show the transformed hexagonal cells in monoclinic symmetry: top, view on *yz* plane; center, view on *xz* plane; bottom, view on *xy* plane.

"central ring" angle of 0°, the corresponding distal bond length c is 1.526 (2) Å (1.532 Å after libration correction).

MNDO calculations performed on the series of spiro compounds **1–6** do not establish the correlation found between the central bond angle α and the length of the distal bond c. However, this method does not establish the correlation found in the experimental values. Such semiempirical methods are mostly inadequate for highly strained molecules, obviously because of the applied neglects and assumptions.[21]

(21) (a) Dewar, M. J. S.; Thiel, W. *J. Am. Chem. Soc.* **1977**, *99*, 4899. (b) Dewar, M. J. S.; Thiel, W. *J. Am. Chem. Soc.* **1977**, *99*, 4907.

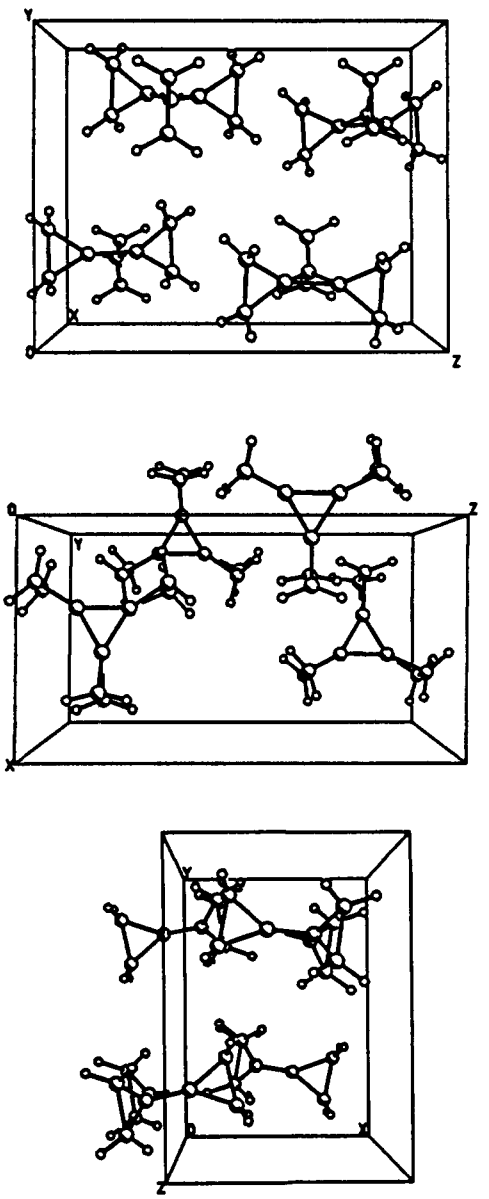

Figure 8. Cell contents of the 96 K LT-phase: top, view on *yz* plane; center, view on *xz* plane; bottom, view on *xy* plane.

(b) X–X Difference Electron Density. Cyclopropane and its derivatives, as far as their stability is concerned, take up a unique position within the series of cycloalkanes. This has recently been reviewed by Cremer.[10] The conventional ring strain energies of cyclopropane and cyclobutane are nearly the same, although the latter should be less strained for geometrical reasons. Ab initio calculations[22] on cyclopropane and cyclobutane with an analysis of the various contributions to the strain energies reveal that the three-membered ring is additionally stabilized by at least 17 kJ/mol. Molecular orbital theory also reveals an exceptional position of cyclopropane. The calculated molecular orbitals as well as the electron density distribution $p(r)$ and its associated Laplace field $\nabla^2 p(r)$ predict an increased electron density in the center of the three-membered ring ("surface delocalization of σ-electrons") and a shift of the point of highest electron density away from the line of the internuclear connection ("bent bond model"). Actually the experimental difference electron densities in the ring centers of **1** are found to be 0.05–0.10 e/Å^3 for the central ring and 0.10–0.15 e/Å^3 for the outer rings. The different values for the central and outer rings are in agreement with the electron distribution model for substituted cyclopropanes proposed by Cremer and Kraka.[19] The maximum for the bond electrons

(22) Cremer, D.; Gauss, J. *J. Am. Chem. Soc.* **1986**, *108*, 7467.

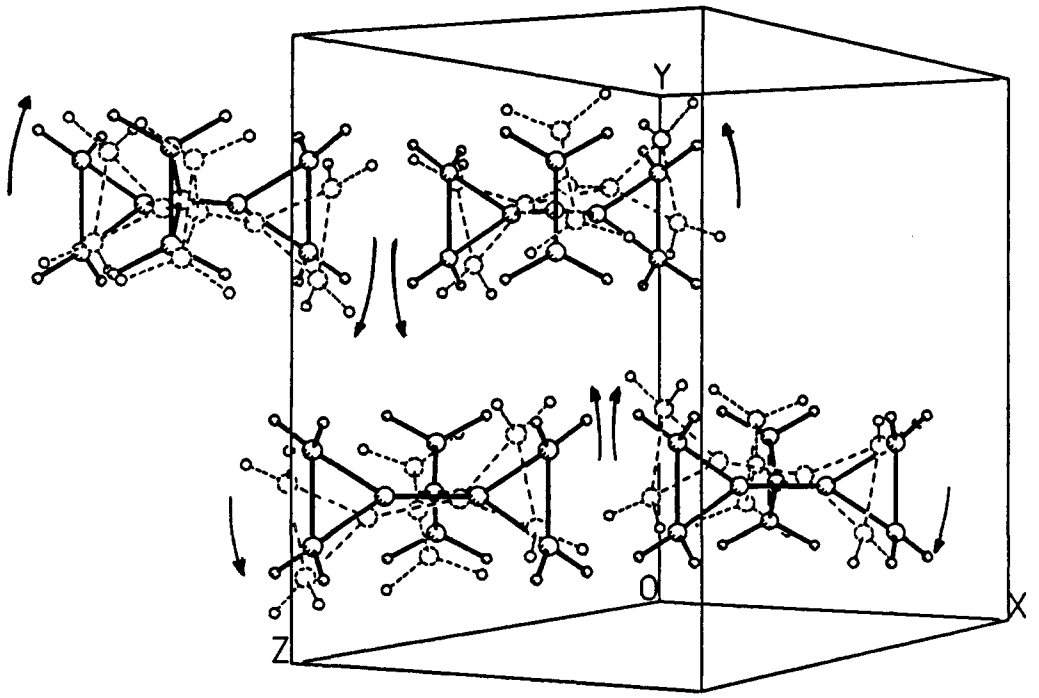

Figure 9. Superpositioning of the 120 K HT- and the 96 K LT-phase (dotted). View direction along the diagonal in the *xz* plane: the arrows indicate the reorientation during the phase transition.

Chart I

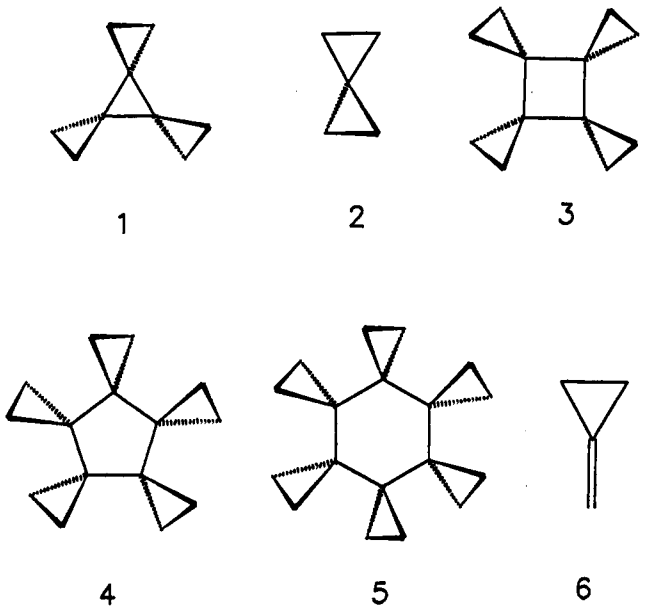

is found to be shifted outside the ring by 0.16 Å for bond a and 0.22 Å for bonds b and c. Stabilization energy and electron delocalization are two arguments leading to the term of σ-aromaticity describing cyclopropane systems. Our experimental observations for the particularly rigid [3]rotane (**1**) support the assumption of surface delocalization of σ-electrons in cyclopropane derivatives and thereby justify one of the necessary, albeit not sufficient, arguments in favor of the concept of σ-aromaticity.[11]

(c) Phase Transition. The solid-state-phase transition of **1** must be considered from a thermodynamic standpoint only, e.g., intermolecular forces, which in this case are restricted to van der Waals contacts, are the driving forces for any change. The HT-phase shows a maximum number of van der Waals interactions. On cooling, cell dimensions as well as the thermal motion amplitudes of molecules decrease. The latter results in an increase of the intermolecular spacing, which in turn lowers the intermolecular attractive forces. Reorientation of the molecules results in a denser packing with a greater number of van der Waals contacts and gain of energy. The increased packing density is reflected in the thermal ellipsoids of the molecules. The HT-phase shows a vibrational mode perpendicular to the layer structure (rigid body motion). In the LT-phase this vibrational mode is lost, thermal ellipsoids are almost spherical, and no preferred direction can be found.

The kinetic process of the phase transition can be derived from changes of the cell dimensions. As can be seen from Figure 4, on cooling the crystal just to above the transition temperature, the *a*- and *c*-axis undergo a sudden significant change, while the *b*-axis remains unchanged (referred to the monoclinic LT-cell). This observation suggests that the axes change in a concerted process which provides space for the tilting of the molecules, as the superimposed structures of the two phases show (Figure 9). The arrows indicate the molecular motion during the phase transition.

Acknowledgment. This work was supported by the Fonds der Chemischen Industrie. T.M. is indebted to the 'Studienstiftung des deutschen Volkes' for a scholarship.

Registry No. [3]Rotane, 31561-59-8.

Supplementary Material Available: Tables of atomic coordinates, thermal parameters, bond lengths, and bond angles of the 220, 200, 140, and 120 K HT-phase and the 96 K LT-phase (26 pages); tables of observed and calculated structure factors (13 pages). Ordering information is given on any current masthead page.